

**Laser pulses for coherent xuv Raman excitation**Loren Greenman,<sup>1,2</sup> Christiane P. Koch,<sup>3</sup> and K. Birgitta Whaley<sup>1,2,\*</sup><sup>1</sup>*Department of Chemistry and Kenneth S. Pitzer Center for Theoretical Chemistry, University of California, Berkeley, Berkeley, California 94720, USA*<sup>2</sup>*Chemical Sciences, Lawrence Berkeley National Laboratory, Berkeley, California 94720, USA*<sup>3</sup>*Theoretische Physik, Universität Kassel, Heinrich-Plett-Straße 40, D-34132 Kassel, Germany*

(Received 9 October 2014; published 13 July 2015)

We combine multichannel electronic structure theory with quantum optimal control to derive femtosecond-time-scale Raman pulse sequences that coherently populate a valence excited state. For a neon atom, Raman target populations of up to 13% are obtained. Superpositions of the ground and valence Raman states with a controllable relative phase are found to be reachable with up to 4.5% population and arbitrary phase control facilitated by the pump pulse carrier-envelope phase. Analysis of the optimized pulse structure reveals a sequential mechanism in which the valence excitation is reached via a fast (femtosecond) population transfer through an intermediate resonance state in the continuum rather than avoiding intermediate-state population with simultaneous or counterintuitive (stimulated Raman adiabatic passage) pulse sequences. Our results open a route to coupling valence excitations and core-hole excitations in molecules and aggregates that locally address specific atoms and represent an initial step towards realization of multidimensional spectroscopy in the xuv and x-ray regimes.

DOI: [10.1103/PhysRevA.92.013407](https://doi.org/10.1103/PhysRevA.92.013407)

PACS number(s): 32.80.Qk, 32.30.Rj, 82.53.Kp

**I. INTRODUCTION**

Multidimensional spectroscopy in the infrared [1] and uv-vis [2,3] spectral regions has proven to be a powerful tool for revealing quantum coherent dynamics in biological systems [4] and quantum devices [5–7]. Extending the techniques of multidimensional spectroscopy to the xuv and x-ray regimes could open the door to studying energy transfer between different atomic sites in molecules [8,9]. It would provide a local probe of valence excitations, which would be invaluable for studies of energy transfer processes in biological systems and quantum devices. However, this presents novel challenges, since the large energy of the xuv and x-ray pulses can result in a high probability of ionization, while selective excitation of a specific intermediate state may be hampered by the presence of a multitude of other states lying close by. On an abstract level, these difficulties reflect the problem of controllability when a continuum of states is involved [10]. Controllability addresses the question whether a quantum control target is reachable, given the properties of the Hamiltonian [11]. For a structureless continuum, no significant controllability is expected, whereas resonances in the continuum are predicted to facilitate control [12], the extent of which depends on the resonance lifetime compared to the duration of the pulses.

Here we combine quantum optimal control theory with the time-dependent configuration-interaction singles (TDCIS) description of electronic structure to calculate experimentally feasible pulse sequences with flexible parameters that coherently excite an xuv Raman excitation on a femtosecond time scale, as an initial step towards multidimensional spectroscopy in the x-ray regime [8]. Achieving such coherent Raman excitation with a high yield is extremely challenging, due to the presence of the ionization continuum that is accessible

by both pump and Stokes pulses. Furthermore, in order to probe electronic dynamics of valence excitations in molecules, it is imperative not only to transfer population into the excited states, but also to have the capability of preparing coherent superpositions of valence states. We seek thus to both drive population to a specific atomic valence excitation *and* achieve a coherent superposition of the ground state and valence excitation with a controllable relative phase. We demonstrate here that use of optimal control theory allows prediction of experimentally feasible pulse forms that populate the desired state up to 13% and achieve superpositions of the ground and excited states with arbitrary relative phase and up to 4.5% excited-state population. This work tackles the problem of an electronic continuum with optimal control, adding an important capability to the growing attempts now under way to tailor multielectron dynamics [13–16].

We consider as a specific example the neon atom, employing the levels shown in Fig. 1. These are accessible in tabletop experiments generating intense high harmonics [17] or using a free-electron laser operating in the xuv regime. A pump pulse of 45.5 eV couples the ground state, with the configuration  $1s^2 2s^2 2p^6$ , to the core-excited resonance  $1s^2 2s^1 2p^6 3p^1$ , driving a  $2s$ - $3p$  particle-hole excitation. A Stokes pulse of 27.0 eV induces the filling of the  $2s$  hole with a  $2p$  valence electron, creating the  $2p$ - $3p$  excitation  $1s^2 2s^2 2p^5 3p^1$ , which is the target valence excited state. Although we do not place any restrictions on the pulse form or frequencies, we use the frequencies mentioned above as the starting point for optimization and find that they remain largely unchanged in the optimization. It is therefore the sequence of the pulses that is the key to avoiding ionization during the time required to achieve the valence excitation, while the generation of coherent superpositions of ground and valence excited states is found to be controlled by the carrier phase envelope of the pump pulse. In Sec. III B we provide a physical interpretation of the mechanism implied by the optimal pulses.

\*whaley@berkeley.edu

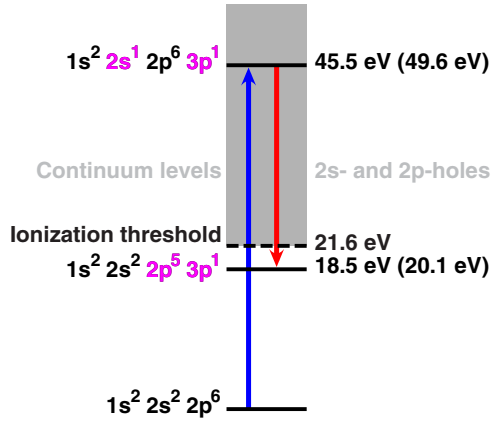


FIG. 1. (Color online) Targeted coherent xuv Raman process in neon. The experimental energies are shown together with TDCIS values in parentheses.

## II. THEORY

### A. Time-dependent configuration-interaction singles method for electronic dynamics including ionization

In order to describe the manifold of excited states and capture the ionizing electron density, we calculate the quantum dynamics using the TDCIS method on a numerical grid with a complex absorbing potential (CAP) [18,19]. The TDCIS method was developed to capture channel coupling in high-harmonic generation [18,20] and it has been used to describe multichannel dynamics in a number of ultrafast processes [21–24]. The wave packet is described by a single-determinant Hartree-Fock ground state  $|\Phi_0\rangle$ , single-particle excitations from an occupied orbital  $i$  to an unoccupied orbital  $a$ ,  $|\Phi_i^a\rangle$ , and time-dependent coefficients  $\alpha$ ,

$$|\Psi(t)\rangle = \alpha_0(t)|\Phi_0\rangle + \sum_{i,a} \alpha_i^a(t)|\Phi_i^a\rangle. \quad (1)$$

The dynamical equations for the coefficients are obtained by inserting Eq. (1) into the Schrödinger equation [18]. A CAP is added to the Hamiltonian in order to capture ionization [18,25,26].

We may simplify the electronic structure calculation by employing a Hartree-Fock-Slater (HFS) one-electron potential as a starting point (TDCIS-HFS). Dynamical calculations with the TDCIS-HFS method are found to yield final-state populations agreeing with the full TDCIS results to within a factor of 3. A further gain in efficiency is possible by using a simplified configuration space including only ionization levels reachable by one-photon absorption within a bandwidth of a few eV (TDCIS-HFS-1P). Pulse sequence optimizations were performed using the TDCIS-HFS-1P method and propagations were performed with the optimal pulses at the full TDCIS level. All calculations employed 1000 grid points in 63.6 Å, with a CAP radius of 42.4 Å and CAP strength of  $10^{-4}$ , with angular momentum functions restricted to  $L \leq 3$ .

### B. Optimal pulse design using Krotov's method

Krotov's optimal control method [27–32] is utilized to find pulses that suppress ionization. It minimizes the cost function

$J$  for the desired excitation

$$J(t_f) = -|\langle \Phi_D | \Psi(t_f) \rangle|^2, \quad (2)$$

where  $|\Phi_D\rangle$  represents the target state (the  $2p$ - $3p$  excitation) and  $\Psi(t_f)$  the time-evolved state in the presence of the external field  $\mathcal{E}(t)$ . The Krotov pulse update formula is given by [32]

$$\mathcal{E}(t)^{(k+1)} = \mathcal{E}(t)^{(k)} - \frac{\lambda}{2S(t)} \text{Im}[\chi(t)^T \mathbf{z} \alpha(t)^{(k+1)}], \quad (3)$$

where  $\mathcal{E}(t)^{(k)}$  is the time-dependent field amplitude at the  $k$ th iteration,  $S(t)$  is an arbitrary shape function that ensures that the pulse goes to zero at the ends of the time propagation,  $\mathbf{z}$  is the transition dipole matrix in the basis of TDCIS states,  $\alpha$  is a vector of the time-dependent coefficients of Eq. (1), and  $\chi$  is the set of corresponding time-dependent covectors [29]. The choice of cost function at the final time determines the initial condition [29]

$$\chi(t_f) = 2\alpha_D[\alpha_D^T \alpha(t_f)]^*. \quad (4)$$

The covectors  $\chi(t)$  are propagated backward in time according to the equations of motion

$$\dot{\chi} = i[\mathbf{H}^T - \mathcal{E}(t)^{(k)} \mathbf{z}^T] \chi(t), \quad (5)$$

with  $\mathbf{H}$  the time-independent part of the Hamiltonian.<sup>1</sup> A derivation of the Krotov update equations including ionization is given in the Appendix.

## III. RESULTS AND DISCUSSION

### A. Obtaining the optimal pulse sequence

Our starting point is a naive pulse sequence for the Raman process obtained by assuming simultaneous, transform-limited (TL) pump  $p$  and Stokes  $S$  pulses  $\mathcal{E}_{p/S}(t) = \mathcal{E}_{0,p/S} \sin[\omega_{p/S}(t - t_{0,p/S}) + \phi_{p/S}] \exp[-4 \ln 2(t - t_{0,p/S})^2 / \sigma_{p/S}^2]$ , with parameters corresponding to the experimental setup of Ref. [17]: a full width at half maximum (FWHM) duration of 2 fs and a peak intensity of  $3.5 \times 10^{12}$  W/cm<sup>2</sup>. This sequence does not populate the Raman state significantly [see Fig. 2(c)]. The overall depopulation of the ground state is small, of order  $10^{-3}$ . This population is divided between  $2p$  holes and the  $2s$  hole. The target state is a particular configuration of the  $2p$  hole that is populated only to a few hundredths of a percent of the total hole population.

Starting with the naive pulse sequence, an optimized sequence is then obtained using Krotov's method. The resulting pulses, shown in Fig. 2(a), achieve the Raman excitation with a population of  $4.4 \times 10^{-2}$ , five orders of magnitude better than the starting pulse. The optimized pulse is increased in amplitude by a factor of about 16 and therefore ionizes more of the electron density. It nevertheless yields an improvement of three orders of magnitude in the percentage contribution of the target state to the total hole probability. The peak intensity of the optimal sequence is about  $7.9 \times 10^{14}$  W/cm<sup>2</sup>. Analysis of the dynamics under the optimized pulse reveals the added

<sup>1</sup>The presence of matrix transposes instead of the usual Hermitian conjugates is due to the use of a CAP.

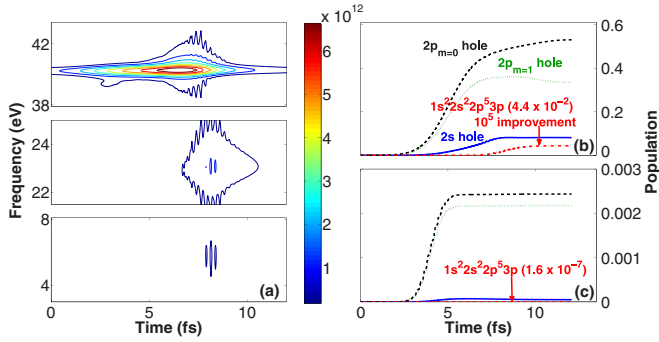


FIG. 2. (Color online) (a) Filtered Wigner distribution of the optimized pulse sequence, showing the Stokes pulse (middle panel) starting at the end of the pump pulse (top panel) and the addition of low-frequency (eV) components (bottom panel). Color bar units are  $\text{W}/\text{cm}^2$ . (b) Populations of  $2p$  and  $2s$  hole states and the target  $1s^2 2s^2 2p^5 3p$  state that are achieved with the optimized pulse. (c) Populations for two simultaneous 2-fs TL pulses with central frequencies of 49.6 and 29.5 eV. The population of the target state (dash-dotted red line) reaches  $4.4 \times 10^{-2}$  for the optimized pulse, compared to  $\sim 1.6 \times 10^{-7}$  for the naive sequence. The  $2p$  holes ( $m = 0$ , black dashed line;  $m = 1$ , green dotted line) correspond to  $1s^2 2s^2 2p^m nl$  configurations and the  $2s$  hole (blue solid line) corresponds to  $1s^2 2s^1 2p^6 nl$  configurations.

low-frequency contribution [bottom panel in Fig. 2(a)] to be irrelevant, whereas the relative timing of the pump and Stokes pulse components are key features. As discussed below, this suggests a sequential mechanism that may be used to further optimize the pulse sequence within experimental constraints.

Coherent superpositions of the Raman state with the ground state are obtained by optimizing with  $0.99e^{i\phi_T}|1s^2 2s^2 2p^5 3p\rangle + 0.16|1s^2 2s^2 2p^6\rangle$  as the target state in the cost function (2), where  $\phi_T$  is the desired relative phase. The target state was empirically determined to drive population to the Raman excited state while maintaining the target phase with the ground state. In this optimization, both the amplitude and phase of the pulse sequence are varied. The procedure enables identification of pulses for arbitrary, prespecified values of the target phase  $\phi_T$ . Figure 3(a) shows the phase error in the target state as a function of  $\phi_T$ . The optimized pulses have a combined peak intensity of about  $10^{14} \text{ W}/\text{cm}^2$  and excite a Raman population of 4.5% while depopulating the ground state by about 53%. Independent of the value of  $\phi_T$ , all optimizations are found to converge on the same pulse envelopes that strongly resemble a time-separated pump and Stokes pair, with the Stokes pulse starting just after the peak of the pump pulse [see Fig. 3(c)]. The optimized pulses differ primarily in the value of the carrier-envelope phase (CEP) of the pump component  $\phi_p$ , calculated using a Hilbert transform of the pulse [33]. It is found to correlate closely with the target phase  $\phi_T$  [see Fig. 3(b)]. The correlation between the target phase and pump CEP implies that the pump imprints its CEP onto the intermediate state to yield the desired relative phase between the intermediate and Raman states. These results show that a coherent superposition can be excited with any desired relative phase  $\phi_T$  merely by changing the pump pulse CEP  $\phi_p$ , once the optimized pulse envelope has been determined.

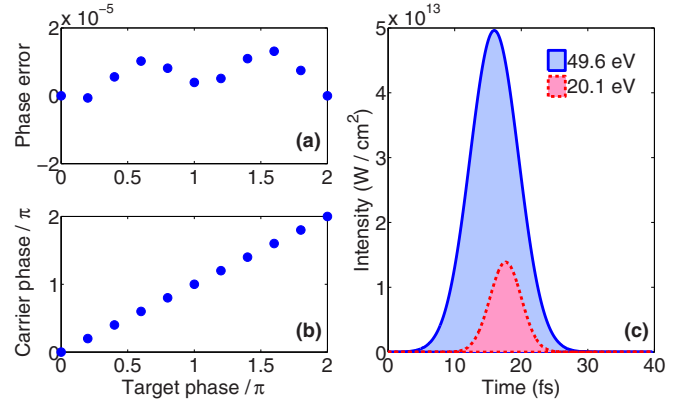


FIG. 3. (Color online) Optimization of coherent superpositions of ground and valence excited states. The phase error (a) and optimized pump pulse carrier-envelope phase  $\phi_p$  (b) are shown as a function of the target phase  $\phi_T$ . Shown on the right (c) is the optimized pulse envelope, showing a clear distinction between the pump (earlier) and Stokes (later) component.

Our optimal control calculations suggest a sequential mechanism whereby first the intermediate state is populated and then the second pulse component acts to transfer population and phase information to the desired state. Exploiting this intuition, the pulse sequences can be engineered further by optimizing each step individually, in order to (i) explore large areas of pulse parameter space for maximum performance or (ii) obtain simple pulses with near-optimal performance that are also consistent with experimental constraints. Varying the parameters of a Gaussian-shaped Stokes pulse starting from the intermediate state, we find complete population transfer to the valence state for a pulse duration of 0.5 fs and a peak intensity of  $2.4 \times 10^{15} \text{ W}/\text{cm}^2$ , corresponding to a pulse energy of  $0.71 \mu\text{J}$  for a spot size diameter of  $10 \mu\text{m}$ . Longer Stokes pulses perform similarly well: complete population transfer is also achieved by 5- and 30-fs pulses with peak intensities of  $3.4 \times 10^{13}$  and  $3.3 \times 10^9 \text{ W}/\text{cm}^2$ , corresponding to powers of 0.10 and  $0.02 \mu\text{J}$ , respectively. Populating the intermediate state efficiently by the pump pulse is thus identified to be the limiting step.

The performance of the pump step is analyzed in Fig. 4 for Gaussian pulses with different pulse durations and energies: At a given energy, the maximum intermediate-state population first increases with pulse duration ( $\sigma \leq 50$  fs) [Fig. 4(a)]. This is explained by a better selectivity of longer, i.e., spectrally narrower, pulses, which avoid populating other resonances nearby. However, for longer pulses, the maximum intermediate-state population decreases due to the lifetime of the intermediate state, which is about 25 fs [34]. Increasing the pulse energy for a given duration [Fig. 4(b)] moves the intermediate-state population maximum to earlier times and achieves larger maxima for a duration of 100 fs. However, for powers less than  $7.1 \times 10^{-1} \text{ mJ}$ , increasing the pulse duration (causing the population maximum to move to a later time) can lead to a decrease in the value of the population maximum [Fig. 4(c)]. The best compromise in terms of pulse power and performance is found for a 50-fs,  $71\text{-}\mu\text{J}$  pulse (with a peak intensity of  $2.4 \times 10^{15} \text{ W}/\text{cm}^2$ ) that achieves a maximum

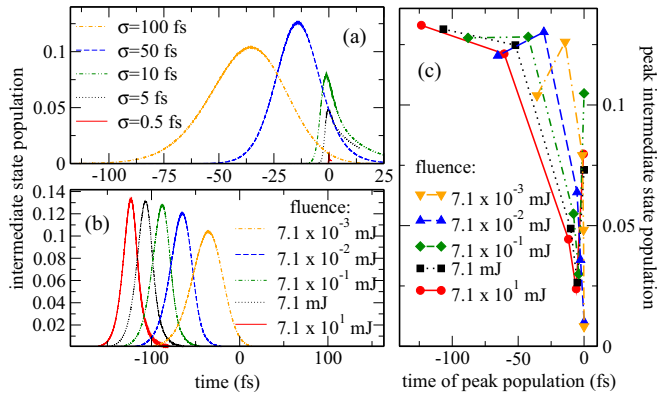


FIG. 4. (Color online) Exploring the performance of Gaussian pump pulses: Intermediate-state population as a function of time ( $t_{0,p} = 0$ ) for (a) different pulse durations at a pulse energy of  $7.1 \mu\text{J}$  and (b) different pulse energies for a FWHM of 100 fs. As the pulse duration increases, larger intermediate-state populations can be achieved, although for a given energy the finite lifetime ( $\sim 25$  fs) acts to drive the intermediate-state population down. (c) Peak intermediate-state population as a function of the time it is achieved for different pulse energies (propagations with the TDCIS-HFS-1P).

intermediate-state population of 0.130, only slightly smaller than the peak at 0.133 seen in Fig. 4(b) for a 100-fs,  $71\text{-mJ}$  ( $1.2 \times 10^{18} \text{ W/cm}^2$ ) pulse.

Improved pulse sequences may now be obtained by setting the time of the Stokes pulse maximum to coincide with the maximum intermediate-state population, using pump pulses that balance the incidental transfer to undesired states with the loss due to the intermediate-state lifetime. An example is shown in Fig. 5 for a 10-fs pump pulse, yielding a Raman state population of 4.5%, compared to the 7.9% maximum intermediate-state population (full TDCIS propagation, added electron correlation now inhibits complete transfer). When increasing the pump duration to 50 fs and keeping the pump energy and Stokes duration and energy fixed, we find final target populations of 13% (using TDCIS-HFS-1P). Such pump pulse parameters are feasible at free-electron laser

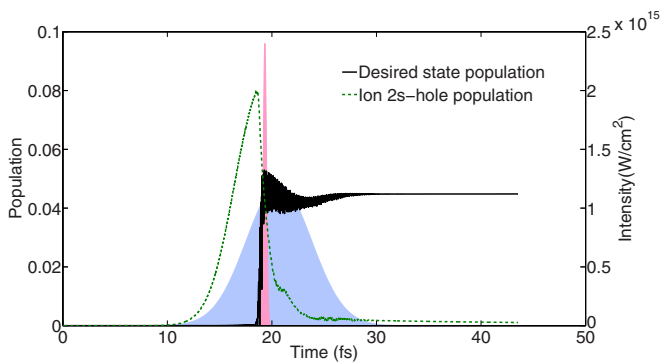


FIG. 5. (Color online) The  $2s$  hole population (dashed green line), corresponding mainly to the intermediate state, and target-state population (solid black line) for a 10-fs,  $7.1\text{-}\mu\text{J}$  pump pulse and a 0.5-fs,  $0.71\text{-}\mu\text{J}$  Stokes pulse centered at 18.7 fs (peak intensities of  $1.2$  and  $2.4 \times 10^{15} \text{ W/cm}^2$ , respectively). Pulse sequences are shown in light blue (pump) and red (Stokes).

(FEL) facilities. While it might prove difficult to realize subfemtosecond Stokes pulses, longer Stokes pulses may be employed instead as discussed above.

## B. Physical analysis of the optimal pulses

Our optimization reveals that an efficient way to achieve valence excitation is to first populate an intermediate resonance state and then transfer that population to the desired valence excitation. The frequencies of this sequential pair of pulses, as expected, correspond to the resonant frequencies of the intermediate and desired states. To achieve the first goal of populating a valence excited state it is therefore the sequence of the pulses that is the main contribution of the optimal control. The timing of the Stokes pulse starting just before the peak of the pump pulse gives the minimal amount of ionization over the time scale for valence excitation. The optimal control calculations also reveal that the phase of the first pump pulse is imprinted on the transient population in the intermediate state, which is then transferred to the Raman state by the Stokes pulse.

The simplicity of our optimal pump-Stokes sequences raises the question of whether other commonly used schemes for Raman transfer perform equally well. In particular, we may compare with both a simultaneous pair of pump and Stokes pulses and a stimulated Raman adiabatic passage (STIRAP) scheme. However, neither of these provides comparable performance, as we now discuss.

The key control of relative timing of pulses is lost with simultaneous pulse pairs and they also do not provide the phase control needed to reach arbitrary superposition states. Nevertheless, simultaneous pulses might be expected to allow generation of a high degree of Raman excitation when the pulse amplitudes are increased. We find, however, that increasing the amplitudes for a set of simultaneous pulses achieves target populations of 0.2% at most, for a pulse intensity of  $10^{16} \text{ W/cm}^2$ , before both ionization and competing population transfer to other states take over and the target populations fall again. The increased intensity of the simultaneous pulses generates significant population in other states and increases background ionization from the  $2p$  orbitals, which is the primary cause of loss in this Raman process. We thus see that the lack of a time delay between pump and Raman pulses does not allow for optimization of the transient intermediate-state population.

In the well-known STIRAP scheme [35] for Raman excitation, the Stokes pulse precedes the pump to avoid population of the intermediate state and thus the detrimental effect of the intermediate-state lifetime. However, in this situation where the intermediate state is a core-excited resonance state, there is only a small coupling between the ground and intermediate states, which results in a very slow adiabatic transfer. In the neon example, we find that valence excitation by a STIRAP scheme is possible only when unrealistically long pulses of hundreds of picoseconds to nanoseconds are employed. Thus, at the femtosecond time scales relevant to xuv pulses, STIRAP pulses cannot adiabatically transfer population.

The optimal pulse sequence is neither concerted (simultaneous) nor adiabatic and instead it selectively populates the intermediate state and depopulates this at the correct time scale to successfully compete with autoionization from the

intermediate state (which has a time scale of about 25 fs [34]). The sequential pulses are therefore the optimal pulse choices for the relevant experimental time scales.

#### IV. CONCLUSION

We have studied the coherent xuv Raman excitation of Ne with shaped pulses and have found that a sequential excitation mechanism proceeding via transient population of an intermediate resonant core-excited state that is then stimulated to emit to the target valence excited state is optimal. We identified the limiting step as population of the intermediate resonance from the ground state. A 50-fs, 71- $\mu$ J pump pulse populates the intermediate state up to 13% and this population can be completely transferred to the Raman state with various Stokes pulses, for example, with a duration of 0.5 fs and an energy of 0.71  $\mu$ J, or 30 fs and 0.02  $\mu$ J. The specific pulses that we find to be optimal at this time scale possess several advantages over the common alternative pulse configuration paradigms for Raman excitation. Thus we showed that simultaneous pulses cannot sufficiently populate the desired states before coupling to the continuum and higher intensities increase background ionization and other competing processes, while the Stokes-pump timing of a conventional STIRAP scheme requires far longer time scales to be adiabatic and does not give rise to the desired excitations on time scales of a few hundred femtoseconds. In contrast, the optimal sequential pulse configurations are effective in transferring significant population from the ground state to the target valence excitation desired states with realistic field amplitudes within these times.

Most important for the realization of coherent multidimensional spectroscopies, the optimal shaped pulse results show that it is possible to excite a superposition of the Raman and ground states with a controllable relative phase. Here the primary control knob is the carrier-envelope phase of the pump pulse. The pulse intensities and durations that we have determined are in principle possible to realize with FELs, in particular with seeded FELs such as FERMI@Elettra that provide the required power and the time resolution to compete with the resonance lifetime [36]. The optimized coherent Raman calculations thus provide design principles for future FELs, especially in regard to the choice of frequencies and phase control, as a prerequisite to implement a multidimensional x-ray spectroscopy scheme.

The sequential pump-Stokes scheme determined from the optimized pulses can readily be applied to other atoms. Indeed, order-of-magnitude estimates of required pulse durations and intensities can be obtained for atoms with isolated resonances, analogous to the  $2s$ - $3p$  resonance utilized here, by comparing the transition dipole strengths with those of neon. More detailed calculations will be required for overlapping resonances, where longer pulses may be required to preferentially address one resonance over the other or where alternate mechanisms for Raman excitation may arise that utilize both (or many) resonances. The mechanism suggested by this example of Raman excitation for neon atoms should also work well for localized valence excitation within molecules, since the intermediate state is localized (atomlike) and driving the population into this state is the limiting step.

With this demonstration of the key elements of state-selective population transfer and excitation of superposition states and the mechanistic insight gained from the optimal shaping of pulses to reach these states, systematic development of coherent multidimensional spectroscopies capable of probing the dynamics of valence excitations in molecules via localized core-hole excitations, such as pump-probe and coherent x-ray Raman scattering (CXRS) [8], now appears feasible. The present work illustrates the usefulness and promise of the coherent control approach in bringing techniques such as CXRS to fruition under the challenging environment of atomic and molecular ionization continua.

#### ACKNOWLEDGMENTS

The authors would like to thank Michael Goerz and Daniel Reich for assistance with the Krotov control code and Stefan Pabst and Robin Santra for help with the XCID TDCIS code. Additionally, we would like to acknowledge Xuan Li, Bill McCurdy, Dan Haxton, Giuseppe Sansone, Ali Belkacem, and Holger Mueller for helpful discussions. We acknowledge computational resources obtained under NSF Grant No. CHE-1048789 and travel assistance provided by NSF international collaboration Grant No. OISE-1158954 and the DAAD. C.P.K. is grateful for financial support from the State Hessen Initiative for the Development of Scientific and Economic Excellence (LOEWE) within the focus project Electron Dynamic of Chiral Systems.

#### APPENDIX: DERIVATION OF THE KROTOV PULSE UPDATE EQUATIONS INCLUDING IONIZATION

We desire to optimize (using the convention of minimization) the overlap of the wave function at some time  $t_f$ ,  $|\Psi(t_f)\rangle$ , with a desired state  $|\Phi_D\rangle$ ,

$$J_{t_f} = -|\langle\Phi_D|\Psi(t_f)\rangle|^2. \quad (\text{A1})$$

If the desired state is a bound state, the symmetric and Hermitian conjugated overlaps should give the same result because the wave function is localized in the CAP-less region and is completely real [as in Eq. (2)]. In order to simplify the derivation, we first use the final time cost function

$$\begin{aligned} J_{t_f} &= -\text{Re}[\langle\Phi_D|\Psi(t_f)\rangle] \\ &= -\frac{1}{2}[\langle\Phi_D|\Psi(t_f)\rangle + \langle\Phi_D|\Psi(t_f)\rangle^*] \\ &= -\frac{1}{2}\{\alpha_D^T\alpha(t_f) + [\alpha_D^T\alpha(t_f)]^*\}. \end{aligned} \quad (\text{A2})$$

We build an optimization functional using the condition in Eq. (A2), as well as a penalty on the distance of the laser pulse from some reference pulse, and a condition that imposes the TDCIS dynamics using Lagrange multipliers  $\chi(t)$  having the same structure as the coefficient vector  $\alpha(t)$  [27,28,30],

$$\begin{aligned} J &= -\frac{1}{2}[\alpha_D^T\alpha(t_f) + \text{c.c.}] \\ &+ \frac{1}{2}\int_0^{t_f}\chi(t)^T\{\dot{\alpha}(t) + i[\mathbf{H} - \mathcal{E}(t)\mathbf{z}]\alpha(t)\}dt + \text{c.c.} \\ &+ \int_0^{t_f}\frac{S(t)}{\lambda}[\mathcal{E}(t) - \mathcal{E}_{\text{ref},t}]^2dt, \end{aligned} \quad (\text{A3})$$

where c.c. denotes the complex conjugate, a superscript  $T$  denotes a transpose,  $S(t)$  is a shape function, and  $\lambda$  is an importance parameter for the energy penalty. Integrating the second line of Eq. (A3) by parts, we obtain

$$\begin{aligned} \bar{J} = & -\frac{1}{2}[\alpha_D^T \alpha(t_f) - \chi(t_f)^T \alpha(t_f) + \chi_0^T \alpha_0 + \text{c.c.}] + \frac{1}{2} \int_0^{t_f} \{-\dot{\chi}(t)^T \alpha(t) + i \chi(t)^T [\mathbf{H} - \mathcal{E}(t)\mathbf{z}]\alpha(t)\} dt + \text{c.c.} \\ & + \int_0^{t_f} \frac{S(t)}{\lambda} [\mathcal{E}(t) - \mathcal{E}_{\text{ref}}(t)]^2 dt. \end{aligned} \quad (\text{A4})$$

We desire an update that would guarantee a monotonically decreasing cost function, so we subtract the cost function at iteration  $k + 1$  from iteration  $k$  [27,28,30],

$$\bar{J}^{(k+1)} - \bar{J}^{(k)} = -\frac{1}{2} \{ \alpha_D^T [\alpha(t_f)^{(k+1)} - \alpha(t_f)^{(k)}] - \chi(t_f)^T [\alpha(t_f)^{(k+1)} - \alpha(t_f)^{(k)}] + \text{c.c.} \} \quad (\text{A5a})$$

$$+ \frac{1}{2} \left( \int_0^{t_f} \{-\dot{\chi}(t)^T [\alpha(t)^{(k+1)} - \alpha(t)^{(k)}] + i \chi(t)^T [\mathbf{H} - \mathcal{E}(t)^{(k)}\mathbf{z}][\alpha(t)^{(k+1)} - \alpha(t)^{(k)}]\} dt + \text{c.c.} \right) \quad (\text{A5b})$$

$$+ \int_0^{t_f} \frac{S(t)}{\lambda} \{ [\mathcal{E}(t)^{(k+1)} - \mathcal{E}_{\text{ref}}(t)]^2 - [\mathcal{E}(t)^{(k)} - \mathcal{E}_{\text{ref}}(t)]^2 \} + \frac{i}{2} \{ [\mathcal{E}(t)^{(k+1)} - \mathcal{E}(t)^{(k)}] \chi(t)^T \mathbf{z} \alpha(t)^{(k+1)} + \text{c.c.} \} dt. \quad (\text{A5c})$$

Equation (A5) can be ensured to be negative by three conditions. First, Eq. (A5a) is forced to be zero by setting  $\chi$  at the final time to be the desired state

$$\chi(t_f) = \alpha_D. \quad (\text{A6})$$

Second, Eq. (A5b) is set to zero by setting the dynamics of  $\chi$ ,

$$\dot{\chi}(t) = i[\mathbf{H}^T - \mathcal{E}(t)^{(k)}\mathbf{z}^T]\chi(t). \quad (\text{A7})$$

Note that Eq. (A7) depends only on the pulse at the  $k$ th iteration  $\mathcal{E}(t)^{(k)}$ . Finally, to obtain an update, we minimize Eq. (A5c) with respect to  $\mathcal{E}(t)^{(k+1)}$  and allow  $\mathcal{E}_{\text{ref}}(t)$  to equal  $\mathcal{E}(t)^{(k)}$  to

obtain

$$\mathcal{E}(t)^{(k+1)} = \mathcal{E}(t)^{(k)} - \frac{\lambda}{2S(t)} \text{Im}[\chi(t)^T \mathbf{z} \alpha(t)^{(k+1)}] \quad (\text{A8})$$

[see Eq. (3)]. Note that the update formula depends on the  $\alpha$  coefficients at the  $(k + 1)$ th iteration and so Eq. (A8) must be solved self-consistently. These update equations are formulated to account for ionization from the CAP in the framework of the TDCIS equations and like the TDCIS equations they use a symmetric overlap rather than a Hermitian overlap. This also leads to backward propagation using a transposed Hamiltonian in Eq. (A7) rather than the Hermitian conjugate.

- 
- [1] D. S. Larsen, K. Ohta, Q.-H. Xu, M. Cyrier, and G. R. Fleming, *J. Chem. Phys.* **114**, 8008 (2001).
- [2] S. Mukamel, *Annu. Rev. Phys. Chem.* **51**, 691 (2000).
- [3] D. M. Jonas, *Annu. Rev. Phys. Chem.* **54**, 425 (2003).
- [4] G. S. Engel, T. R. Calhoun, E. L. Read, T.-K. Ahn, T. Mančal, Y.-C. Cheng, R. E. Blankenship, and G. R. Fleming, *Nature (London)* **446**, 782 (2007).
- [5] X. Li, T. Zhang, C. N. Borca, and S. T. Cundiff, *Phys. Rev. Lett.* **96**, 057406 (2006).
- [6] M. Erementchouk, M. N. Leuenberger, and L. J. Sham, *Phys. Rev. B* **76**, 115307 (2007).
- [7] L. Yang and S. Mukamel, *Phys. Rev. B* **77**, 075335 (2008).
- [8] S. Tanaka and S. Mukamel, *Phys. Rev. Lett.* **89**, 043001 (2002).
- [9] S. Mukamel, D. Abramavicius, L. Yang, W. Zhuang, I. V. Schweigert, and D. V. Voronine, *Acc. Chem. Res.* **42**, 553 (2009).
- [10] M. Shapiro and P. Brumer, *Quantum Control of Molecular Processes* (Wiley Interscience, New York, 2012).
- [11] D. D'Alessandro, *Introduction to Quantum Control and Dynamics* (Chapman & Hall/CRC, Boca Raton, 2007).
- [12] V. Zeman, M. Shapiro, and P. Brumer, *Phys. Rev. Lett.* **92**, 133204 (2004).
- [13] T. Klamroth, *J. Chem. Phys.* **124**, 144310 (2006).
- [14] M. Mundt and D. J. Tannor, *New J. Phys.* **11**, 105038 (2009).
- [15] A. Castro, J. Werschnik, and E. K. U. Gross, *Phys. Rev. Lett.* **109**, 153603 (2012).
- [16] X. Li, C. W. McCurdy, and D. J. Haxton, *Phys. Rev. A* **89**, 031404 (2014).
- [17] T. K. Allison, T. W. Wright, A. M. Stooke, C. Khurmi, J. van Tilborg, Y. Liu, R. W. Falcone, and A. Belkacem, *Opt. Lett.* **35**, 3664 (2010).
- [18] L. Greenman, P. J. Ho, S. Pabst, E. Kamarchik, D. A. Mazziotti, and R. Santra, *Phys. Rev. A* **82**, 023406 (2010).
- [19] S. Pabst, L. Greenman, and R. Santra, XCID program package for multichannel ionization dynamics, Rev. 629, with contributions from P. J. Ho. DESY, Hamburg, Germany, 2011.
- [20] S. Pabst, L. Greenman, D. A. Mazziotti, and R. Santra, *Phys. Rev. A* **85**, 023411 (2012).
- [21] S. Pabst, L. Greenman, P. J. Ho, D. A. Mazziotti, and R. Santra, *Phys. Rev. Lett.* **106**, 053003 (2011).
- [22] A. Wirth, M. T. Hassan, I. Grguraš, J. Gagnon, A. Moulet, T. Luu, S. Pabst, R. Santra, Z. Alahmed, A. Azzeer *et al.*, *Science* **334**, 195 (2011).

- [23] S. Pabst, A. Sytcheva, A. Moulet, A. Wirth, E. Goulielmakis, and R. Santra, *Phys. Rev. A* **86**, 063411 (2012).
- [24] A. Sytcheva, S. Pabst, S.-K. Son, and R. Santra, *Phys. Rev. A* **85**, 023414 (2012).
- [25] A. Goldberg and B. W. Shore, *J. Phys. B* **11**, 3339 (1978).
- [26] R. Santra and L. S. Cederbaum, *Phys. Rep.* **368**, 1 (2002).
- [27] D. Tannor, V. Kazakov, and V. Orlov, in *Time-Dependent Quantum Molecular Dynamics*, edited by J. Broeckhove and L. Lathouwers (Plenum, New York, 1992), pp. 347–360.
- [28] J. Somló, V. A. Kazakovski, and D. J. Tannor, *Chem. Phys.* **172**, 85 (1993).
- [29] A. I. Konnov and V. F. Krotov, *Automat. Rem. Contr.* **60**, 1427 (1999).
- [30] A. Bartana, R. Kosloff, and D. J. Tannor, *Chem. Phys.* **267**, 195 (2001).
- [31] J. P. Palao, R. Kosloff, and C. P. Koch, *Phys. Rev. A* **77**, 063412 (2008).
- [32] D. Reich, M. Ndong, and C. P. Koch, *J. Chem. Phys.* **136**, 104103 (2012).
- [33] J. Duoandikoetxea and D. Cruz-Urbe, *Fourier Analysis* (American Mathematical Society, Providence, (RI) 2001).
- [34] K. Codling, R. P. Madden, and D. L. Ederer, *Phys. Rev.* **155**, 26 (1967).
- [35] K. Bergmann, H. Theuer, and B. W. Shore, *Rev. Mod. Phys.* **70**, 1003 (1998).
- [36] <http://www.elettra.trieste.it/FERMI>.